Torque Ripple Minimization of PMSM using Adaptive Feedback Linearization based Direct Torque Control

R. Suja[1], P. Subha Karuvelam[2]

[1]Associate Professor, Department of Electrical and Electronics Engineering, PET Engineering College, Vallioor, Tamil Nadu, India.

[2]Assistant Professor, Department of Electrical and Electronics Engineering, Government College of Engineering, Tirunelveli, Tamil Nadu, India.

Sujapet1976@gmail.com

Abstract

The electronic computation of PMSM generates torque ripples and undesirable harmonics which negatively impacts the smooth speed operation and efficiency of PMSM. This paper proposes a combined Feedback Linearization based Direct Torque Control methodology for Impedance Source Inverter (ZSI) to mitigate torque ripples and undesirable harmonics of PMSM. The proposed controller mitigates torque ripples and undesirable harmonics by changing the desired switching pattern by generating reference voltages for three-phase ZSI in stationary reference frame using torque and flux as input. The advantage of combining proposed control scheme and ZSI is that it boosts the inversion operation and reduces the requirement of the DC-DC converter in boosting. Therefore, the conversion efficiency can be increased by 4-8 %. The performance of the proposed control scheme is studied by subjecting PMSM to full load torque and under load disturbances. The obtained results show the ability and effectiveness of the proposed control scheme in comparison with the conventional DTC method.

Keywords: Permanent magnet synchronous motor, Feedback linearization, Direct torque control, Impedance source inverter, Space vector pulse width modulation.

1. Introduction

In this fast-paced world, Permanent Magnet Synchronous Motors (PMSM) are well known for its high power, robustness, simple structure and effective operation, and has been commonly used in industrial automation applications. The PMSM drive is electronically commutated and operated through power electronic converter [1]. In olden days, electronic commutation of PMSM was performed using volt/frequency control and field oriented control [2-4]. However, when PMSM drives are excited through power electronic Voltage Source Inverter (VSI) or Current Source Inverter (CSI) and field oriented control; it produces torque ripples and undesirable harmonics [5-7]. This possibly creates a negative impact on the speed control of PMSM and affects the overall efficiency of the PMSM drive [8].

Recently, several approaches are adopted for the reduction in torque ripple and mitigation of undesirable harmonics. Torque ripples can be mitigated either by hardware adaptation or by modifying the control strategy of a PMSM converter controller. In [9, 10], VSI is made up of power electronic switches and their control strategies are obtained by means of PWM, SPWM, and SVPWM etc. Therefore, by modifying the control strategy of PMSM, the torque ripple and undesirable harmonics can be mitigated. In [11], various types of rectifier schemes for a grid utility interface of variable frequency drives have been proposed. However, it has some disadvantages like; high ripples in torque as well as flux and variable switching frequency. In [12], the harmonic distortion level for converter fed motor drive is decreased by the higher order rectifier. This method can quickly and effectively limit the load angle within the stable range but produces an unsatisfactory performance when load angle changes. Traditional Impedance Source Inverter (ZSI) based strategy has been proposed [13, 14]. ZSI has a DC source on its two sides and switching control of ZSI is carried out by the PI control strategy. The limitations of traditional VSI and Current CSI are overcome by ZSI. The control strategy is effective, but the generated input power for PMSM operation is insufficient and therefore makes the inductor current to ripple [15].

In order to overcome these issues, the modified control strategy for converter control has been proposed in [16-20]. Torque ripple minimization of PMSM using a digital observer controller has been proposed [16]. The Digital observer controller uses measured speed to generate i_d and i_q as a reference signal. It has been noted that the torque ripple factor is reduced to 50% only for full load disturbance by using digital observer controller strategy. Input-output feedback linearization based control strategy has been proposed [17] to minimize the torque ripple in PMSM. This method doesn't show effective

minimization as it eliminates only particular order of harmonics. Direct Torque Control (DTC) strategy has been proposed in [18-20] for mitigation of torque ripple and undesirable harmonics. DTC strategy uses motor flux and torque as control variables. Usually, DTC strategy is adopted with six-switch 3ϕ VSI or CSI power electronic inverter. But, due to the susceptibility of such power electronic inverter, fault commonly occurs and affects the performance of the PMSM drive.

In order to overcome the above-mentioned problems, this paper proposes an adaptive combined Feedback Linearization based Direct Torque Control (FBL-DTC) methodology for an impedance source inverter to mitigate the torque ripples and undesirable harmonics of the PMSM drive. The torque ripple in a PMSM drive is caused by d-axis, q-axis currents and flux linkage of the permanent magnet. As the developed torque T_m is directly proportional to the phase current, the *q*-axis current can be reduced by regulating the switching frequency of the ZSI, the PMSM drive is set to operate at a constant current. The proposed controller generates a reference voltage for ZSI in stationary reference frame using calculated torque and flux variables and maintains constant current which in turn operates the PMSM at rated torque. The proposed control strategy not only mitigates torque ripples and undesirable harmonics but also boosts the inversion operation. Therefore the requirement of the DC-DC converter for boosting is eliminated and the conversion efficiency is increased by 4-8%. The dynamic performance of the proposed control scheme is validated using MATLAB/Simulink software and verified using hardware prototype.

2. Study system description

The system considered for the study is shown in Figure 1. The study system consists of a PMSM connected to a DC source through ZSI. The parameters of PMSM taken for the study are given in the appendix. ZSI switching pulses are generated by the proposed adaptive FBL-DTC strategy and the system has been subjected to load variation by shedding the load after 0.05 s in-order to evaluate the performance of the proposed control strategy. Furthermore, the system consists of speed sensor to measure the motor speed during analysis. The measured speed is possessed by the proposed adoptive FBL-DTC and SVPWM to generate control signals to the ZSI.

3. Dynamic modeling of the PMSM

To evaluate the performance of the proposed control strategies, PMSM is modeled in detail using stator circuit electrical equations in d–q coordinates and is given as [21],

$$v_d = \frac{d\varphi_d}{dt} + R_s i_d - \omega\varphi_q \tag{1}$$

$$v_q = \frac{d\varphi_q}{dt} + R_s i_q + \omega\varphi_d \tag{2}$$

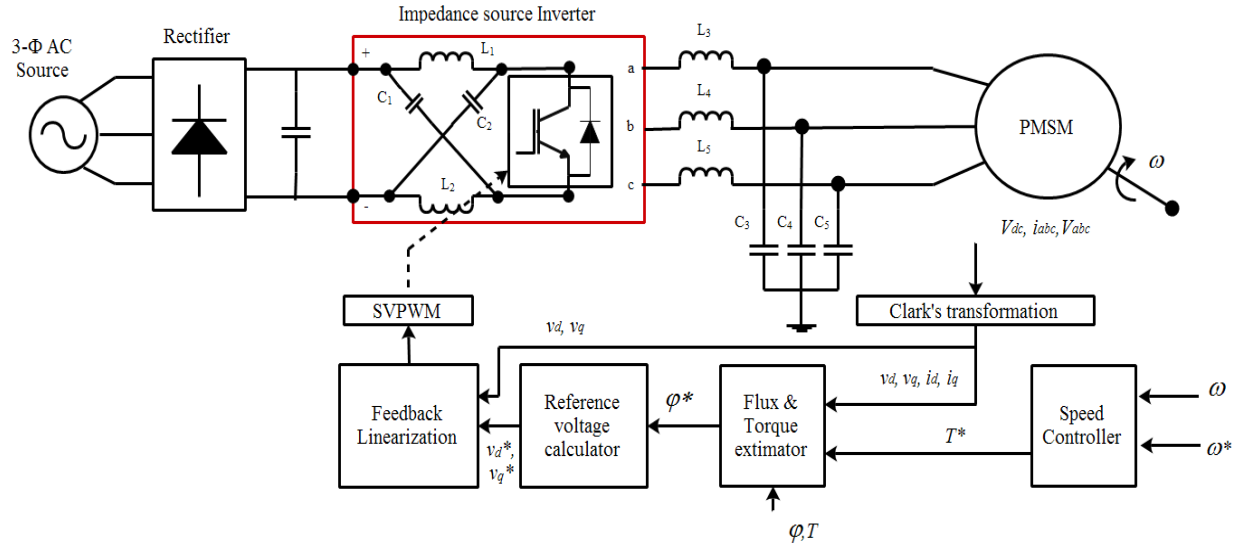

Figure 1. Block diagram of the torque ripple minimization using FBL-DTC strategy

Where, R_s is the stator resistance, $v_{d\ and}$ i_d are the d-axis voltage and current, φ_d is the d-axis flux linkage, $v_{d\ and}$ i_q are the q-axis voltage and current respectively, φ_q is the q-axis flux linkage, respectively [22]. Further, the flux linkage of *d-q* axis is expressed in *d-q* coordinates as follows,

$$\varphi_d = L_d i_d + \varphi_m \tag{3}$$

$$\varphi_q = L_q i_q \tag{4}$$

Where L_d is the d-axis inductance, φ_m is the permanent magnet flux linkage, L_q is the q-axis inductance. There is no permanent magnet flux linkage in q-axis, as the magnetic axis is aligned along with only d-axis. Consequently, as d-q coordinates of the motor move along with the rotor, the inductance of the stator is independent of time in this system [23]. The mechanical movement of the PMSM is represented by mechanical equation and is given as,

$$T_e = \frac{Jd\omega}{dt} + T_L + B\omega \tag{5}$$

where, T_e is the electromagnetic torque of the motor, T_L is the load torque, J represents the moment of inertia, ω is the rotor speed and B is the friction co-efficient, respectively. From equation (5), the rotor speed increases until there is a positive difference between the motor torque and the load torque. Further, the acceleration of the motor depends on the moment of inertia and friction co-efficient. The torque equation is expressed with d-q magnitudes, and is given as,

$$T_e = 1.5P(\varphi_d i_q - \varphi_q i_d) \tag{6}$$

Where P represents the number of pole pairs in rotor. The motor torque equation is obtained with respect to the magnetic flux linkage and d-q axis current is given as,

$$T_e = 1.5P(\varphi_m i_q - (L_q - L_d) i_d i_q) \tag{7}$$

When L_d is equal to L_q, the motor torque only depends upon the i_q and the equation is give as,

$$T_e = 1.5P\varphi_m i_q \tag{8}$$

Further, the cogging torque of PMSM is given as,

$$T_{cog} = -0.5P\varphi_g^2 \frac{dR}{d\theta} \tag{9}$$

Where, R is the air-gap reluctance, φ_g represents air-gap flux linkage and θ represents the angle position of the rotor (Jing et al., 2004).

The PMSM in d-q coordinate form is re-written in the state space model with respect to rotor reference frame and is given as,

$$\begin{pmatrix} i_d^* \\ i_q^* \\ \omega^* \end{pmatrix} = \begin{pmatrix} -(r/L_d) & 0 & 0 \\ 0 & (-r/L_q) & (-\varphi_m/L_q) \\ 0 & (\varphi_m/2H) & (-B/H) \end{pmatrix} \begin{pmatrix} i_d \\ i_q \\ \omega \end{pmatrix} + \begin{pmatrix} (1/L_d) & 0 \\ 0 & (1/Lq) \\ 0 & 0 \end{pmatrix} \begin{pmatrix} v_d \\ v_q \end{pmatrix} + \begin{pmatrix} \omega_s \omega_r i_q \\ -\omega_s \omega_r i_d - (\Delta\varphi_m/L_q)\omega_r \\ -(T_L/2H) + (\Delta\varphi_m/2H) i_d \end{pmatrix} \tag{10}$$

Where, H is the field intensity of the motor drive, ω_s and ω_r are the stator and rotor speed, respectively. The state space equation of the model is given by placing the state variable as X, control input as Y and output as Z,

$$X = (i_d \quad i_q \quad \omega_r)^T \tag{11}$$

$$Y = (v_d \quad v_q)^T \tag{12}$$

$$Z = (i_d \quad i_q)^T \tag{13}$$

The equation's (11), (12) and (13) is rewritten as,

$$\overset{*}{X} = AX + BY + f(x) \tag{14}$$

and the output equation is given as,

$$Z = CX \tag{15}$$

Where, $f(x)$ represents the function of system formed by the nonlinearity and the uncertainties of the system, which has to be persistent in x to subsist [21, 22].

4. Dynamic modeling of the Impedance Source Inverter

The schematic diagram of a 3-ϕ ZSI is shown in Figure 2. The ZSI network consists of two indistinguishable inductances and two indistinguishable capacitances connected in a precise manner to attain preferred study system as shown in Figure 1. In this study, Shoot through boost control strategies of ZSI is considered [24]. An additional switch is employed in anti-parallel to the input diodes for eliminating the discontinuous inductor current originating during undesirable operating modes. Therefore, from the Figure 2, we have I_{L1}=I_{L2} and V_{C1}=V_{C2}. Further, the peak inverter output voltage $\hat{V}_i$ of the Z network is given as,

$$\hat{V}_i = V_{dc}/1-2D_0 = b_f.V_{dc} \quad (16)$$

Where D_0 is the shoot-through time duty ratio, b_f is the booting factor and V_{dc} is the dc input voltage [25, 26]. The state space equation of z network for shoot-through mode can be written as,

$$\begin{bmatrix} L\frac{dI_{L1}}{dt} \\ L\frac{dI_{L2}}{dt} \\ C\frac{dV_{C1}}{dt} \\ C\frac{dV_{C2}}{dt} \end{bmatrix} = \begin{bmatrix} -(r_c+r_L) & 0 & 1 & 0 \\ 0 & -(r_c+r_L) & 0 & 1 \\ 0 & -1 & 0 & 0 \\ -1 & 0 & 0 & 0 \end{bmatrix} \begin{bmatrix} I_{L1} \\ I_{L2} \\ V_{C1} \\ V_{C2} \end{bmatrix} \quad (17)$$

Where, r_C represents the load capacitive reactance and r_L represents the load inductive reactance, respectively. The Z source network capacitor voltage $V_{c1\ and}\ V_{c2}$ is determined by

$$V_{c1} = V_{c2} = V_c = \frac{1-D_0}{1-2D_0}V_0 \quad (18)$$

From the above equation (18) it is clear that the V_c is less than V_0, which implies that a high Z source capacitor voltage stress. Hence, the Z source network inductor current equals the average input current [27]. Furthermore, the Z source capacitive current decreases with the increase in inductor current. The Z source ripple current has been expressed as,

$$\Delta I_{L1} = \Delta I_{L2} = \Delta I_L = \frac{(1-D_0)\tau V_0}{L} = \frac{D_0(1-D_0)}{1-2D_0}\frac{\tau V_0}{L} \quad (19)$$

5. Proposed Feedback Linearization based Direct Torque Control strategy

In this section, a novel FBL based DTC approach is evolved for the purpose of controlling ZSI fed PMSM drive. The FBL technique is well known for its most effective control over the nonlinear dynamic systems. FBL allows the developer to utilize a linear control approach by algebraically converting the nonlinear system into a partially or fully modeled linear system. The proposed FBL technique differs completely from the conventional linearization technique. Here, the FBL control is attained by utilizing the feedback terms rather than the linear approximation terms. In the study system, the FBL-DTC strategy generates the reference space vector for a PMSM drive. The FBL-DTC strategy uses T_e and φ as the state variables to control the system input v_d and v_q.

The FBL-DTC strategy estimates the flux and torque variables using the measured voltage and current of the PMSM. The estimated flux and torque variables are used to generate voltage vectors for triggering the ZSI. By adding up a feedback linearization loop along with the conventional DTC, it has an added advantage of increased smooth speed control over the drive. The block diagram of the proposed approach is shown in Figure 3. In the proposed FBL-DTC strategy, ZSI output voltage v_{abc}, line current i_{abc} and DC input voltage v_{dc} are measured with respect to the 3-ϕ bridge rectifier using voltage and current sensors. The measured v_{abc}, i_{abc} and v_{dc} are transformed to d-axis and q-axis component using Clark's transformation [27].

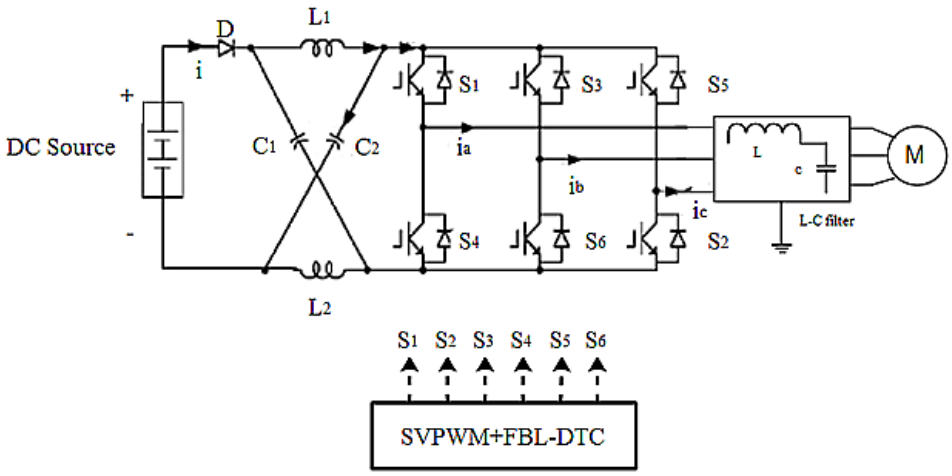

Figure 2. Impedance source inverter circuit diagram

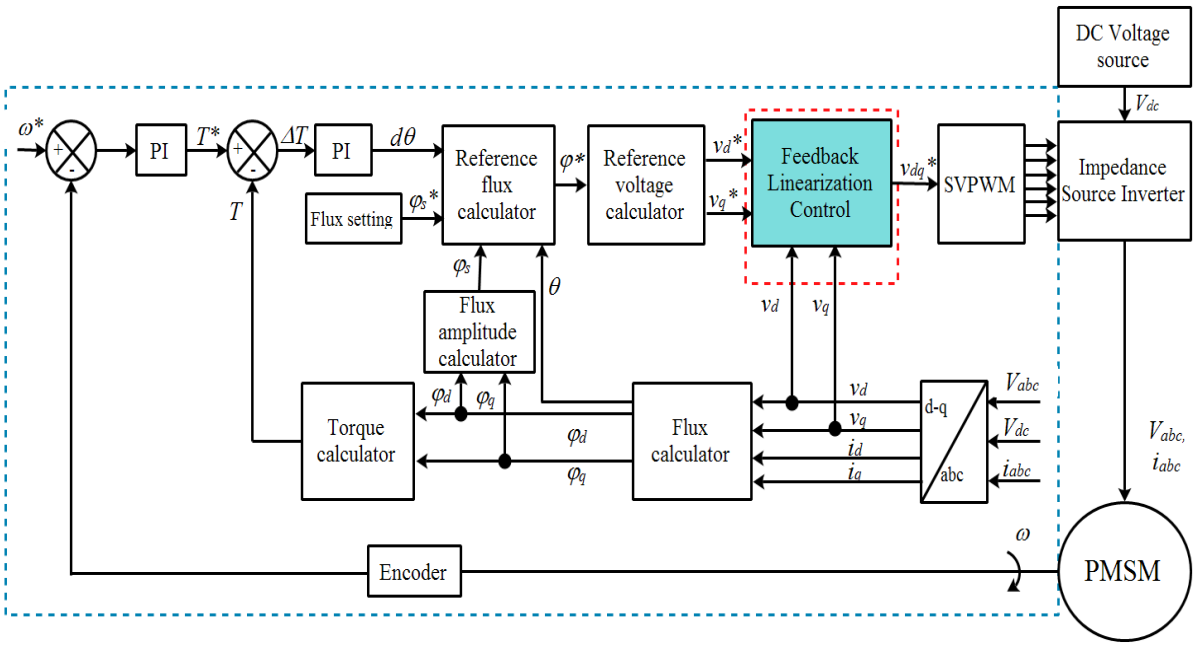

Figure 3. Adaptive FBL-DTC strategy control circuit

The estimated *d*-axis and *q*-axis component of stator input voltage and current, is used for calculating stator flux φ_d and φ_q and the equation is given as,

$$\varphi_d = \int (v_d - i_d R_s) dt \tag{20}$$

$$\varphi_q = \int (v_q - i_q R_s) dt \tag{21}$$

Where *Rs* is the stator resistance. After calculating φ_d and φ_q the overall all stator flux φ_s is estimated using a flux amplitude calculator [28, 29]. Furthermore, the estimated φ_d and φ_q is fed into torque calculator and torque is calculated as,

$$T = \frac{3p}{4}(\varphi_d i_q - \varphi_q i_d) \tag{22}$$

Where ω is the speed of the PMSM measured using speed sensors. After estimating the values of φ_s, T and ω they are set to compare with their reference values ω^*, φ_s^* and T^*; respectively. The proposed approach consists of two PI controllers for controlling the torque and speed. Initially, the speed error is processed by one of the PI controllers to generate T^* and the torque error is processed by the other PI controllers to generate reference angle $d\theta$. The role of DTC is to generate voltage command v_d^* and v_q^* using the following variables φ_s^*, φ_s, $d\theta$ and θ. The PI controller plays a vital role in the proposed control strategy. The PI controllers gain values are tuned by means of Ziegler–Nichols method. The K_P and K_I value obtained for the speed loop PI controller is 10 and 0.4 respectively and for the torque control loop, the PI controller is 18.3 and 3 respectively. The generated voltage command v_d^* and v_q^* and measured stator input voltage v_d and v_q is processed through the feedback linearization control loop. The role of FBL loop is to generate an accurate reference voltage command to the SVPWM. The FBL control block checks the response to the given initial condition.

$$v'_{dq} = -Ke^*_{v_{dq}} - e_{v_{dq}} \tag{23}$$

If the response is not acceptable, the FBL control adjusts the reference value until the closer value is obtained.

$$v''_{dq} = -2Ke^*_{v_{dq}} - e_{v_{dq}} \tag{24}$$

The generated voltage reference is fed to the SVPWM. The working and generation of switching pattern using SVPWM are referred to [10]. The FBL-DTC strategy suppresses the generated torque by regulating the motor torque in opposite to the produced torque ripple by electronic commutation. The proposed approach boosts up the inversion operation by reducing the complexity in generating command signals. Therefore, the requirement of the

DC-DC converter for boosting is eliminated and conversion efficiency is increased by 4-8%.

6. Results and Discussion

6.1. Simulation results

To evaluate the performance of the proposed FBL-DTC methodology, a profound simulation study has been carried out using the study system described in section 2. In this study, the system is subjected to full load test and load shedding disturbances. This study mainly focuses on torque ripple minimization and undistorted harmonic elimination. Therefore, results related to those alone have been comparatively discussed between conventional DTC and proposed FBL-DTC scheme.

Initially, the PMSM is started at full load of 22 N-m and operated by means of the conventional DTC strategy. The load is set to shed by 10 N-m after 0.25 s and the speed of the motor starts to vibrate as shown in Figure 4(a). The corresponding torque waveform has been shown in Figure 4(b). It is observed that the ripples appear in the torque and the torque ripple factor is 83%. The corresponding stator current i_d and i_q are shown in Figure 5(a). It can be noted that the stator current decreases along with the shedding of the load at 0.25 s and high noise are present due to ZSI-pulse width modulation. Figure 5 (b) and (c) shows the measured stator and rotor flux of PMSM using conventional DTC. It is observed that the sudden shedding of load leads the stator and rotor flux to saturate. It takes nearly 0.35 s to settle and regain its normal operation. Figure 6(a) shows the flux vector phasor representation and rotor flux angle obtained using conventional DTC strategy. It is noted that due to uncertainty, the rotor angle falls below the reference value. Figure 7(a) shows the uncertain harmonic of the PMSM stator current. It is observed that the stator current has a harmonic of 3.47%.

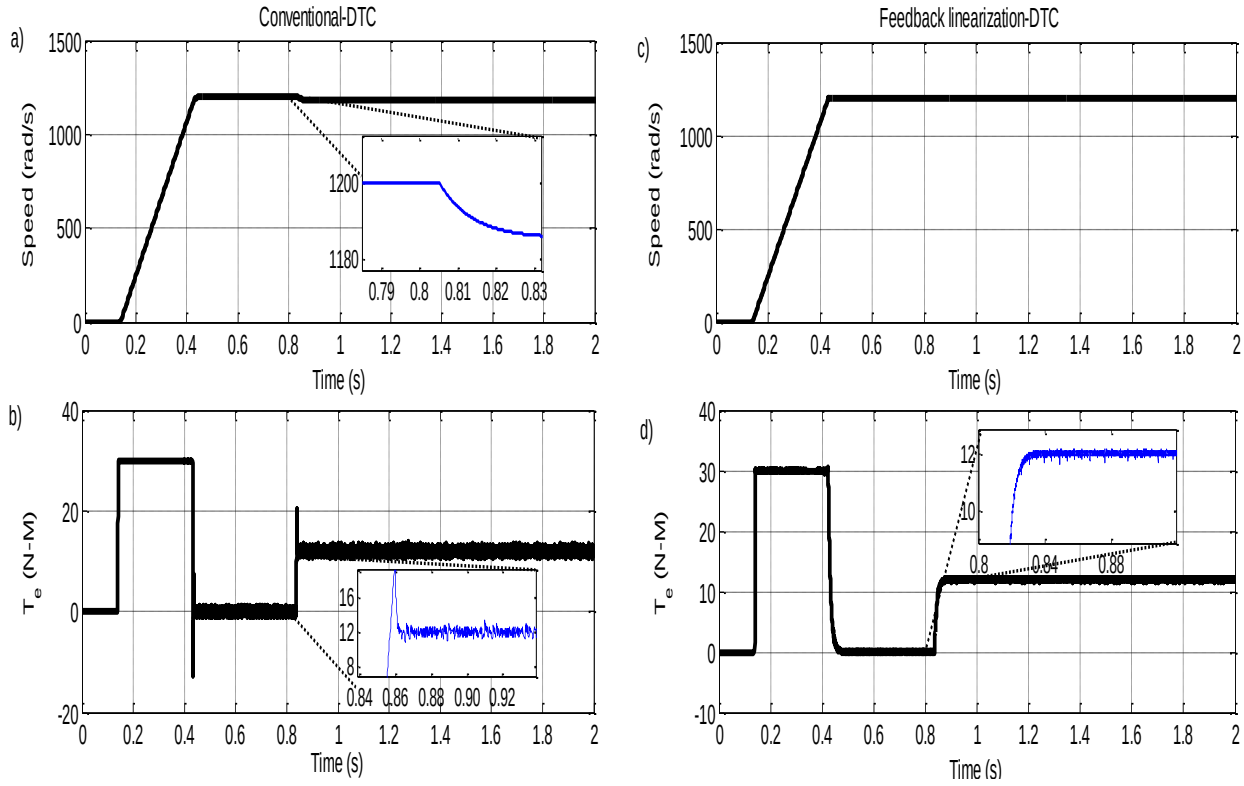

Figure 4. Performance evaluation of PMSM ; (a) Speed in rad/s using conventional DTC, (b) Torque in N-m using conventional DTC, (c) Speed in rad/s using FBL-DTC, (d) Torque in N-m using conventional FBL-DTC.

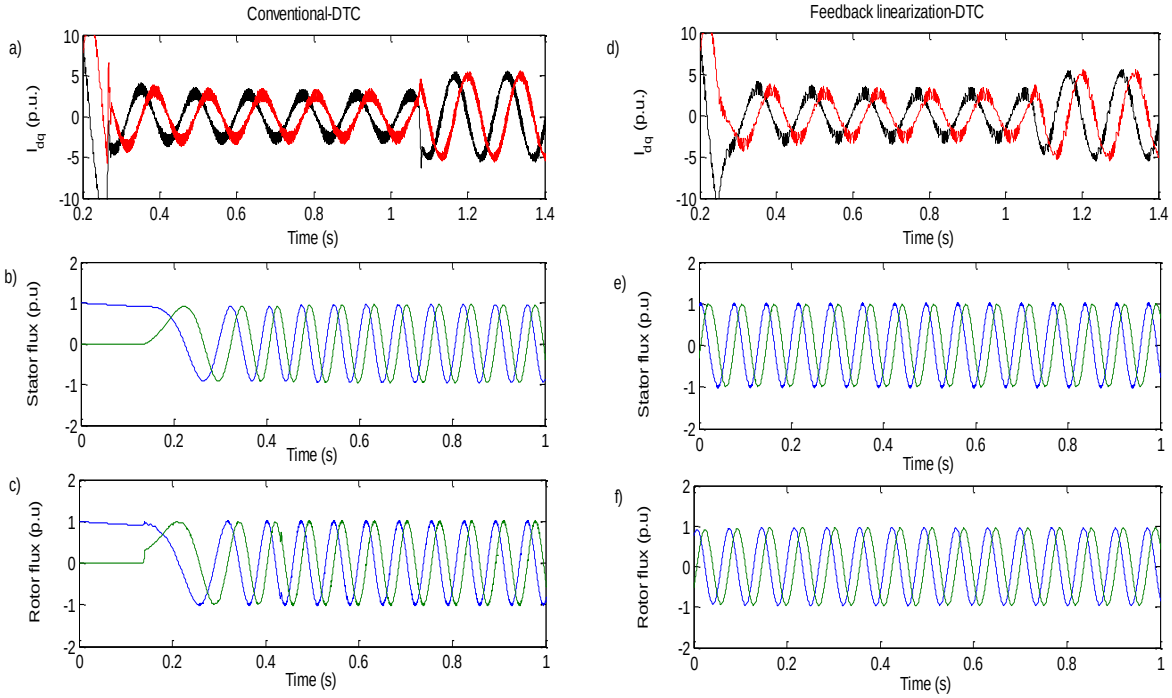

Figure 5. PMSM analysis of; (a) Stator current idq using conventional DTC, (b) Stator flux using conventional DTC, (c) Rotor flux using conventional DTC, (d) Stator current idq using FBL-DTC, (b) Stator flux using FBL-DTC, (c) Rotor flux using FBL-DTC

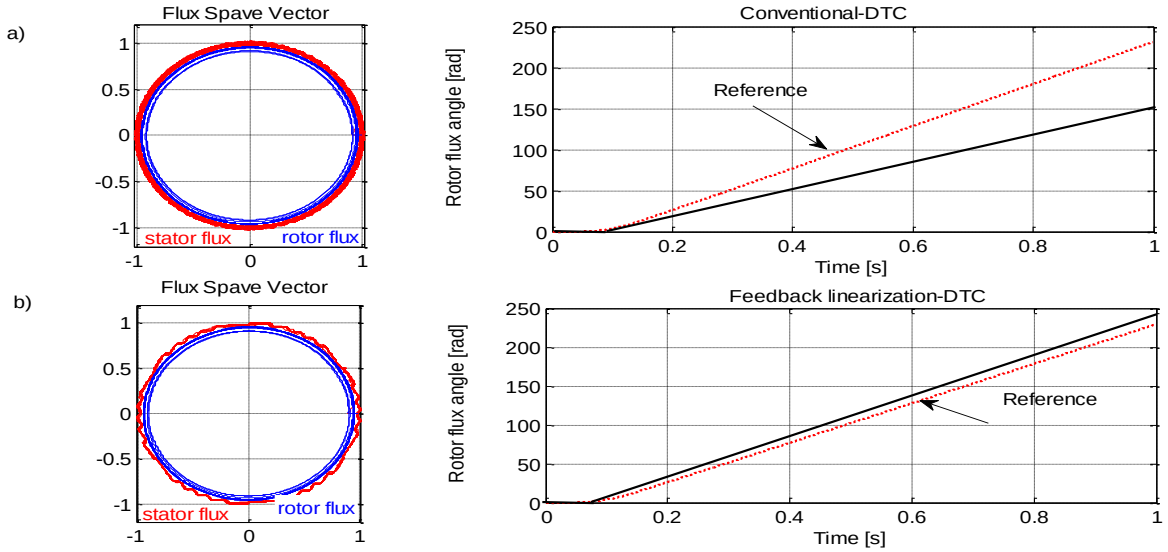

Figure 6. Flux space vector and Rotor flux angle; (a) Using conventional DTC, (b) using FBL-DTC

In the next stage, PMSM is started at a full load of 22 N-m and operated by means of the proposed FBL-DTC strategy. Similarly, the load is set to shed by 10 N-m after 0.25 s and corresponding speed is measured and presented in Figure 4(c). It is observed that the speed maintains constant without vibration at 1200 rad/s. The feedback linearization control checks the vd and vq variables and thereby generates desired switching pulse using SVPWM to regulate and obtain the preferred speed thereby the torque ripples are minimized. Figure 4(d) shows the torque of the PMSM obtained using proposed FBL-DTC strategy. It is observed that the level of torque ripple factor is 66 %, which is comparatively less than conventional DTC strategy. Figure 5(d) shows the d and q component of the stator current. It is

observed that stator current decreases due to the variation of load and stabilizes faster by 0.2 s when compared to the conventional DTC strategy. Further, the noise level of stator current is also reduced when compared with the conventional control strategy.

Figure 5(e) and 5(f) shows the calculated stator and rotor flux of PMSM using proposed FBL-DTC. From the figure, it is observed that the stator and rotor flux stabilizes faster when compared with the conventional DTC strategy. Figure 6 (b) shows the flux vector phasor representation and the rotor flux angle obtained using proposed FBL-DTC strategy. It is noted that the uncertainty is overcome by the proposed FBL-DTC and PMSM produces the angle equal to the reference value. Figure 7 (b) shows the uncertain harmonic of the PMSM stator current. It is observed, the stator current has a harmonic of 1.21 %, which is comparatively lesser than the conventional control strategy. It can be observed from the simulation result that proposed FBL - DTC strategy based PMSM drive significantly works effectively with reduced torque and undesirable harmonics. To validate these simulation results, hardware implementation has been carried out which is being discussed in successive section.

6.2. Experimental validation

To validate the proposed FBL-DTC strategy, an experimental is carried out using the experimental setup as shown in Figure 8. The parameters of experimental setup are listed in the appendix. The experimental setup consists of PMSM coupled to a DC generator, where the DC-generator is loaded by different resistive load and is driven by a SVPWM 3-ϕ impedance source inverter. The 3- ϕ impedance source inverter is made of IGBT and cross impedance sources and is powered by a DC supply of 220 V. The input and output commands are passed from system to experimental setup through an dSPACE DS1104 kit.

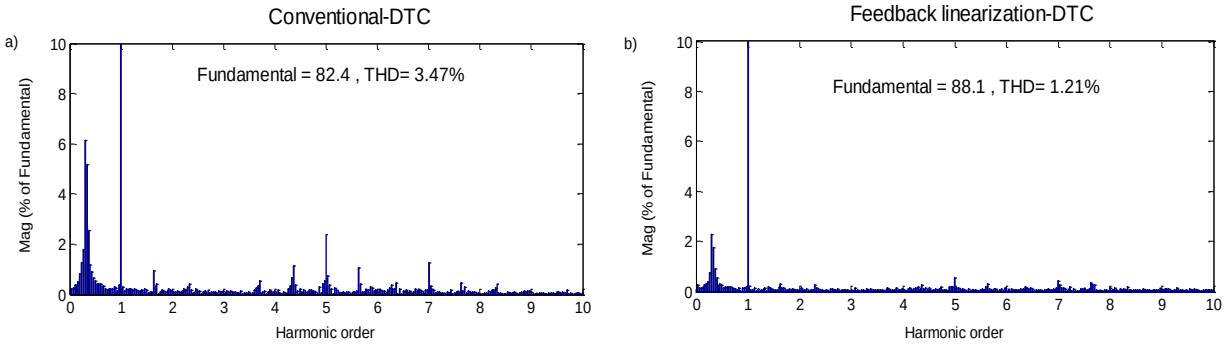

Figure 7. Harmonic analysis PMSM line current; (a) after using conventional DTC, (b) after using FBL-DTC

Figure 8. Experimental setup

The setup also consists of torque meter and speed encoder, for continuous monitoring of the torque and speed of the PMSM. The result obtained from the experimental study has been presented in Figures (9-15). Figure (9) shows the speed response of the PMSM obtained using conventional DTC with high noise in the waveform and the speed settles with the reference with a delay and Figure (10) shows the speed response of the PMSM obtained using proposed FBL-DTC. It can be seen that the noise level in speed has been reduced and no overshooting takes place in curve using FBL-DTC when compared to conventional DTC. The results observed from the analysis are listed in table 1. From the table, it can be noted that the proposed FBL-DTC strategy settles faster for both speed and torque when compared to conventional DTC strategy.

Figure (11) shows the torque response of PMSM using conventional DTC, it is observed that the torque ripples are high and torque drops during the variation in speed and during loading. Figure (12) shows the torque response of PMSM using FBL-DTC, it is observed that the torque ripples have been considerably reduced and smooth torque has been obtained using FBL-DTC strategy. Figure (13), (14) and (15) shows the measured back emf, line current and line current- THD of the PMSM. Form figure 16 it can be observed that the THD level is lesser when compared with the conventional DTC. It can be observed from the experimental results, that the proposed FBL - DTC strategy based PMSM drive significantly works effectively with reduced torque and undesirable harmonics.

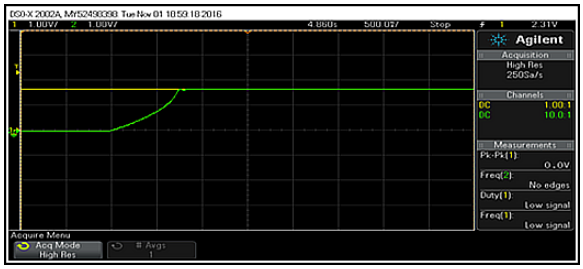

Figure 9. The speed response of PMSM using the conventional DTC

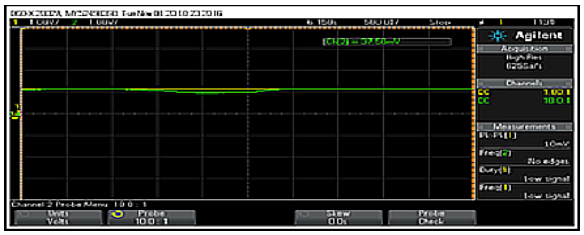

Figure 10. The speed response of PMSM using the FBL-DTC

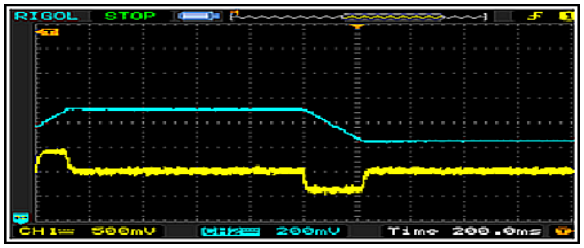

Figure 11. Measured torque of PMSM using the conventional DTC

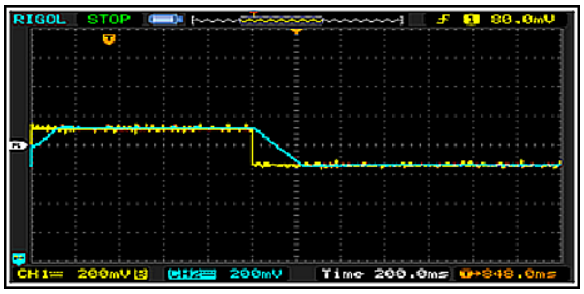

Figure 12. Measured torque of PMSM using the FBL-DTC

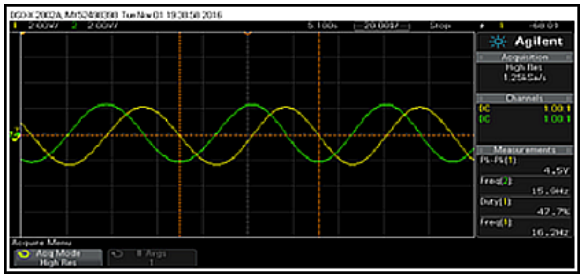

Figure 13. Measured PMSM Back EMF

Table 1. Comparative analysis

Strategy / Parameters	Proposed FBL-DTC strategy		Conventional DTC strategy	
	Simulation	**Experiment**	**Simulation**	**Experiment**
Stator flux ripple (wb)	0.03	0.11	0.075	0.18
Torque ripple (Nm)	0.07	0.19	0.15	0.43
Settling time of speed (ms)	13.77	24.3	34.3	52.5
Settling time of torque (ms)	5.25	13.3	11.0	29.6
THD line current	1.21	1.2	3.47	4.3

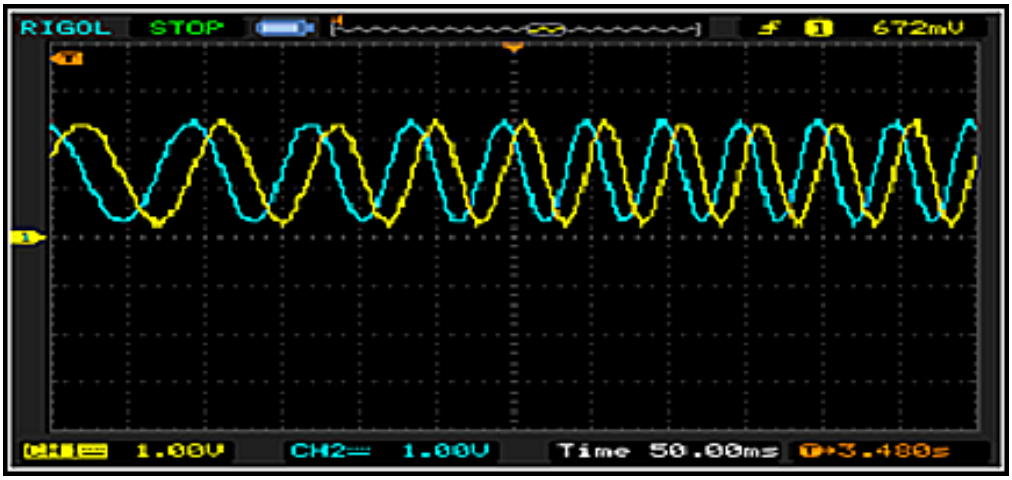

Figure 14. Measured i_d and i_q of the PMSM

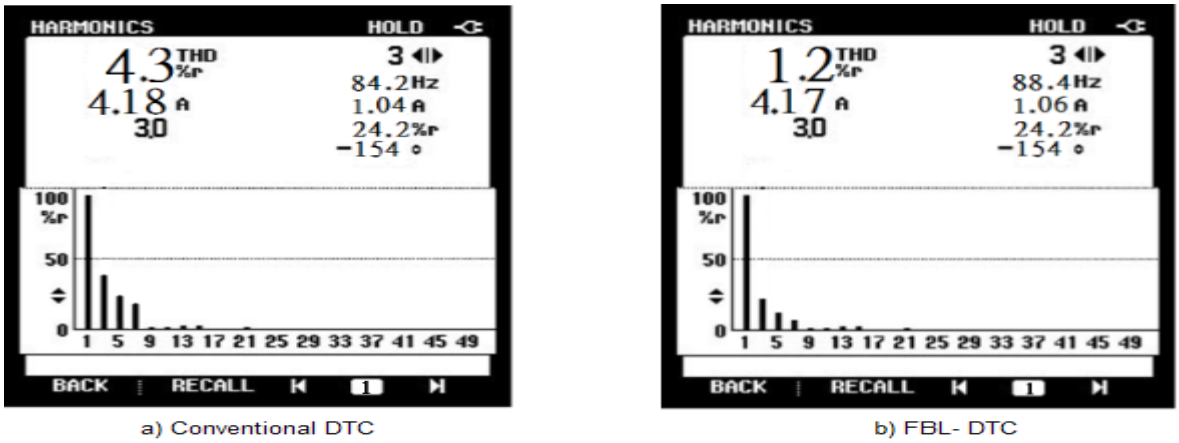

a) Conventional DTC b) FBL- DTC

Figure 15. Measured THD of line current

7. Conclusion

A novel method for torque ripples and undesirable harmonics minimization of the PMSM drive using adaptive combined Feedback Linearization based Direct Torque Control methodology is presented in this paper. The performance of the proposed FBL-DTC methodology is evaluated by an extensive simulation and an experimental study, carried out on PMSM under various load conditions. The results show that the proposed FBL-DTC strategy is proficient in reducing torque ripples and eliminating undesirable harmonics of PMSM. The obtained simulation and experimental results also prove the ability and effectiveness of the proposed FBL-DTC scheme compared to conventional DTC method.

Acknowledgement

This research received no specific grant from any funding agency in the public, commercial, or nonprofit sectors. Further, the authors would like to thank the authorities of PET Engineering College, Vallioor and Government College of Engineering, Tirunelveli, Tamilnadu India, for their support given to do this research work.

Appendix

Parameters of the system considered for the study,

PMSM motor parameters: Number of pole pairs, P = 4, Moment of inertia, J = 0.0008 Kg-m^2, Stator resistance, R_s= 0.15Ω, Phase winding inductance, *Ls* = 0. 25 mH, d-axis inductance, L_d = 0.0085 H, q-axis inductance, Lq = 0.0085 H, Magnetic flux, φ = 0.175 Wb, Speed, N = 2500 Rpm, Stator current, i_s = 3.5 A, DC voltage, V_{DC} = 90 V, Back-EMF constant = 0.028 v/rad/s.

DC Generator parameters: Power = 250 W, Voltage = 24 V_{DC}, Nominal current = 13.5 A, Rated speed = 2750 Rpm

Impedance Source Inverter parameters: AC input voltage = 230 V, Inductance, L1 = L2 = 1.6 mH, Capacitance, C1 = C2 = 1000 μF

Reference

1. Pillay, P. and Krishnan, R., 1989. Modeling, simulation, and analysis of permanent-magnet motor drives. I. The permanent-magnet synchronous motor drive. IEEE Transactions on industry applications, 25(2), pp.265-273.
2. Zhong, L., Rahman, M.F., Hu, W.Y. and Lim, K.W., 1997. Analysis of direct torque control in permanent magnet synchronous motor drives. IEEE Transactions on Power Electronics, 12(3), pp.528-536.
3. Tang, L., Zhong, L., Rahman, M.F. and Hu, Y., 2004. A novel direct torque controlled interior permanent magnet synchronous machine drive with low ripple in flux and torque and fixed switching frequency. IEEE Transactions on power electronics, 19(2), pp.346-354.
4. Islam, R., Husain, I., Fardoun, A. and McLaughlin, K., 2009. Permanent-magnet synchronous motor magnet designs with skewing for torque ripple and cogging torque reduction. IEEE Transactions on Industry Applications, 45(1), pp.152-160.
5. Holtz, J. and Springob, L., 1996. Identification and compensation of torque ripple in high-precision permanent magnet motor drives. IEEE Transactions on Industrial Electronics, 43(2), pp.309-320.
6. Tang, L., Zhong, L., Rahman, M.F. and Hu, Y., 2003. A novel direct torque control for interior permanent-magnet synchronous machine drive with low ripple in torque and flux-a speed-sensorless approach. IEEE Transactions on industry applications, 39(6), pp.1748-1756.
7. Sun, T., Kim, J.M., Lee, G.H., Hong, J.P. and Choi, M.R., 2011. Effect of pole and slot combination on noise and vibration in permanent magnet synchronous motor. IEEE Transactions on magnetics, 47(5), pp.1038-1041.
8. Corley, M.J. and Lorenz, R.D., 1998. Rotor position and velocity estimation for a salient-pole permanent magnet synchronous machine at standstill and high speeds. IEEE Transactions on Industry Applications, 34(4), pp.784-789.
9. Maamoun, A., Alsayed, Y.M. and Shaltout, A., 2010. Space-vector pwm inverter feeding a permanent-magnet synchronous motor. World Academy of Science, Engineering and Technology, 41, pp.627-631.
10. Pradeep, K., Mandeep, K. and Surender, D., 2015. Sensor less speed control of PMSM using SVPWM technique based on MRAS method for various speed and load variations. Lecture Notes in Engineering and Computer Science, 2217(1), pp.375-380.
11. Al-Nabi, E., Wu, B., Zargari, N.R. and Sood, V., 2012. Input power factor compensation for high-power CSC fed PMSM drive using d-axis stator current control. IEEE Transactions on Industrial Electronics, 59(2), pp.752-761.
12. Filip, Ioan, and Iosif Szeidert. "Adaptive fuzzy PI controller with shifted control singletons." Expert Systems with Applications 54 (2016): 1-12.
13. Liu, P. and Liu, H.P., 2012. Permanent-magnet synchronous motor drive system for electric vehicles using bidirectional Z-source inverter. IET Electrical Systems in Transportation, 2(4), pp.178-185.
14. Ping, L.I.U. and He-ping, L.I.U., 2011. Application of z-source inverter for permanent-magnet synchronous motor drive system for electric vehicles. Procedia Engineering, 15, pp.309-314.
15. Gulez, K., Adam, A.A. and Pastaci, H., 2008. Torque ripple and EMI noise minimization in PMSM using active filter topology and field-oriented control. IEEE Transactions on Industrial Electronics, 55(1), pp.251-257.
16. Hasanien, H.M., 2010. Torque ripple minimization of permanent magnet synchronous motor using digital observer controller. Energy Conversion and Management, 51(1), pp.98-104.
17. 17. Boroujeni, M.S., Markadeh, G.A. and Soltani, J., 2017. Torque ripple reduction of brushless DC motor based on adaptive input-output feedback linearization. ISA transactions. http://dx.doi.org/10.1016/j.isatra.2017.05.006i
18. Inoue, Y., Morimoto, S. and Sanada, M., 2012. Comparative study of PMSM drives systems based on current control and direct torque control in flux-weakening control region. IEEE Transactions on Industry Applications, 48(6), pp.2382-2389.
19. Zhang, Y. and Zhu, J., 2011. A novel duty cycle control strategy to reduce both torque and flux ripples for DTC of permanent magnet synchronous motor drives with switching

frequency reduction. IEEE Transactions on Power Electronics, 26(10), pp.3055-3067.

20. 20. Zhang, Y., Zhu, J., Xu, W. and Guo, Y., 2011. A simple method to reduce torque ripple in direct torque-controlled permanent-magnet synchronous motor by using vectors with variable amplitude and angle. IEEE Transactions on Industrial Electronics, 58(7), pp.2848-2859.

21. Chen, X., Hu, J., Chen, K. and Peng, Z., 2016. Modeling of electromagnetic torque considering saturation and magnetic field harmonics in permanent magnet synchronous motor for HEV. Simulation Modelling Practice and Theory, 66, pp.212-225.

22. Li, S., Liu, H. and Ding, S., 2010. A speed control for a PMSM using finite-time feedback control and disturbance compensation. Transactions of the Institute of Measurement and Control, 32(2), pp.170-187.

23. Kapun, A., Čurkovič, M., Hace, A. and Jezernik, K., 2008. Identifying dynamic model parameters of a BLDC motor. Simulation Modelling Practice and Theory, 16(9), pp.1254-1265.

24. Peng, F.Z., 2003. Z-source inverter. IEEE Transactions on industry applications, 39(2), pp.504-51.

25. Sitharthan, R. and Geethanjali, M., 2017. An adaptive Elman neural network with C-PSO learning algorithm based pitch angle controller for DFIG based WECS. Journal of Vibration and Control, 23(5), pp.716-730.

26. Huang, Y., Shen, M., Peng, F.Z. and Wang, J., 2006. $ Z $-Source Inverter for Residential Photovoltaic Systems. IEEE Transactions on Power Electronics, 21(6), pp.1776-1782.

27. Faiz, J. and Mohseni-Zonoozi, S.H., 2003. A novel technique for estimation and control of stator flux of a salient-pole PMSM in DTC method based on MTPF. IEEE Transactions on Industrial Electronics, 50(2), pp.262-271.

28. Zheng, P., Zhao, J., Liu, R., Tong, C. and Wu, Q., 2010. Magnetic characteristics investigation of an axial-axial flux compound-structure PMSM used for HEVs. IEEE Transactions on Magnetics, 46(6), pp.2191-2194.

29. Martínez-Béjar, R., Cadenas, J.M., Shirazi, H. and Compton, P., 2009. A semantics-driven, fuzzy logic-based approach to knowledge representation and inference. Expert Systems with Applications, 36(2), pp.1940-1960.